

Patterns

Multivariate landscapes constructed by Bayesian estimation over five hundred microbial electrochemical time profiles

Highlights

- A high-throughput bioelectrochemical device parallelly runs 1920 chronoamperometry
- SD remained less than 10%, with 96 standalone electrochemical cells
- Bayesian estimation was applied to 576 time profiles of microbial current production
- High performance of riboflavin at negative potential was mechanically validated

Authors

Waheed Miran, Wenyuan Huang, Xizi Long, Gaku Imamura, Akihiro Okamoto

Correspondence

okamoto.akihiro@nims.go.jp

In brief

Data science is an innovative approach to optimizing complex biological power generation operating conditions. However, technology capable of delivering large amounts of high-quality training data is essential for its practical use. Here, we developed an electrochemical device that achieves more than hundreds of times higher output than conventional ones for constructing a high-quality database. The data-driven discovery of a high-performance electron transfer mechanism under unexplored conditions verifies the effectiveness of our approach to integrating data science and microbial electrochemistry.



Article

Multivariate landscapes constructed by Bayesian estimation over five hundred microbial electrochemical time profiles

 Waheed Miran,^{1,2} Wenyuan Huang,^{1,3} Xizi Long,¹ Gaku Imamura,^{1,4} and Akihiro Okamoto^{1,3,5,*}
¹International Center for Materials Nanoarchitectonics, National Institute for Materials Science, 1-1 Namiki, Tsukuba, Ibaraki 305-0044, Japan

²School of Chemical and Materials Engineering, National University of Sciences and Technology, Islamabad 44000, Pakistan

³Graduate School of Chemical Sciences and Engineering, Hokkaido University, North 13 West 8, Kita-ku, Sapporo, Hokkaido 060-8628, Japan

⁴Graduate School of Information Science and Technology, Osaka University, 1-2 Yamadaoka, Suita, Osaka 565-0871, Japan

⁵Lead contact

 *Correspondence: okamoto.akihiro@nims.go.jp
<https://doi.org/10.1016/j.patter.2022.100610>

THE BIGGER PICTURE Commercial bioelectrochemical systems (BESs) require breakthroughs at the scientific and engineering levels. Although BESs can be used to realize cleaner energy, effective waste treatment, and environmental remediation, technology rollout is hampered by their low efficiency and a lack of optimum working conditions. Machine-learning solutions can be used for the optimization of BESs; however, their implementation is hindered by several challenges, such as low-throughput systems and lack of electrolyte- and potentiostatic-independent operation in high-throughput systems with high reproducibility. A rational design of high-throughput systems with the application of data science for performance enhancement is of vital importance to BES research. Our high-throughput platform capable of generating low deviation datasets with electrolyte and potentiostatic standalone cells, coupled with data science, could help in progress in fundamental electromicrobiology research and advancing the successful commercialization of BESs.



Proof-of-Concept: Data science output has been formulated, implemented, and tested for one domain/problem

SUMMARY

Data science emerges as a promising approach for studying and optimizing complex multivariable phenomena, such as the interaction between microorganisms and electrodes. However, there have been limited reports on a bioelectrochemical system that can produce a reliable database until date. Herein, we developed a high-throughput platform with low deviation to apply two-dimensional (2D) Bayesian estimation for electrode potential and redox-active additive concentration to optimize microbial current production (I_c). A 96-channel potentiostat represents <10% SD for maximum I_c . 576 time- I_c profiles were obtained in 120 different electrolyte and potentiostatic conditions with two model electrogenic bacteria, *Shewanella* and *Geobacter*. Acquisition functions showed the highest performance per concentration for riboflavin over a wide potential range in *Shewanella*. The underlying mechanism was validated by electrochemical analysis with mutant strains lacking outer-membrane redox enzymes. We anticipate that the combination of data science and high-throughput electrochemistry will greatly accelerate a breakthrough for bioelectrochemical technologies.

INTRODUCTION

Electroactive bacteria that perform extracellular electron transfer (EET) to/from electrodes show great potential for applications in

the fields of energy and environmental sustainability, including power generation from wastewater, bioremediation, chemical production, and amperometric biosensors.^{1,2} With increasing demand for commercialization,³ various strategies are being



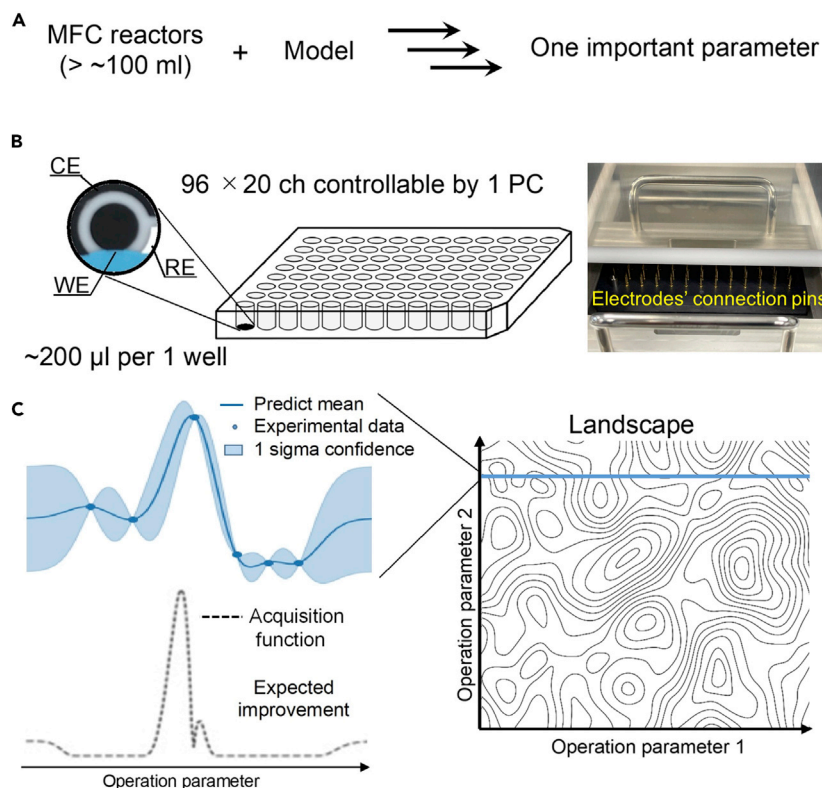


Figure 1. Approaches for reaction optimization

(A) Mechanistic studies enable systematic identification of important parameters.

(B) Developed high-throughput electrochemical system that operates single-potential amperometry in 96-well plate with printed working electrode (WE), counter electrode (CE), and reference electrode (RE). WE and CE are carbon, and RE is Ag/AgCl electrode.

(C) Graphic outline of Bayesian optimization for two parameters. 1D example depicting a Gaussian process surrogate model fitted to data collected from objective and the corresponding expected utility surface, which is maximized to select the optimum condition. The solid line and the shaded area represent the mean of prediction and one-sigma confidence interval, respectively.

tion system and an analysis platform for massive time-current profile data.

In this study, we developed a high-throughput potentiostat system with 96-well plates with silk-screen-printed electrodes that was applied to landscape the redox mediator concentration and electrode potential constructed from 576 time profiles of microbial current production (Figures 1B and 1C). One of the most important controllable factors for BES performance is the type and concentration of the redox mediator.²³ External redox

adopted to improve and optimize the performance of bioelectrochemical systems (BESs), including reactor configurations and varying operating conditions, electrode material development, and additives based on fundamental EET mechanisms.^{4–9} However, understanding the complexity of BESs, which includes elucidation of the interactions between different impactful parameters (Figure 1A) and control of microbial electrochemical catalysis, requires breakthroughs at the scientific and engineering levels. Data science shows potential for capturing the landscape of such complex systems from limited databases. However, the effective use of data science in BESs has been a challenge, as they require a massive dataset with defined parameters and high reproducibility, referred to as a “high-quality database.” The less controlled experimental aspects, while obtaining large data from manual experiments, often cause serious reproducibility concerns, which restrict the consensual knowledge gain. Hence, a high-quality database is the core area for applying data science to experimental studies.^{10–13} However, although significant development has been achieved in high-throughput BESs, there are no reports on a system that can achieve enough reproducibility while simultaneously controlling the following three parameters for each reactor: potential, electrolyte, and microorganism, which are critical for BES performance.^{14–19} Furthermore, appropriate data processing algorithms for dealing with a large volume of current-time profile data have not been established yet.¹⁸ Therefore, even in the most recent studies, the use of data science for the number of datasets used for training the model are very limited, at nine.^{20–22} The foundation for applying data science to BESs still requires two innovations: a high-quality data collec-

mediators play a vital role in enhancing the electron transfer between bacteria and the electrode.^{24,25} The performance of mediators may be considerably different depending on their redox potential, diffusion constant of shuttling electron mediators, and ability to bind with bacterial membrane enzymes.^{26,27} Furthermore, the electrode potential can modify global gene regulation and metabolic pathways in electrogenic bacteria. Therefore, microbial current production may be beyond our physicochemical understanding of the EET mechanism, which is suitable for application in data science. We used *Shewanella oneidensis* MR-1 to compare the impact of variables, different mediators (riboflavin [RF], flavin mononucleotide [FMN], 2-hydroxy-1,4-naphthoquinone [HNQ], anthraquinone-1,5-disulfonate [AQDS]), the concentration of mediators (1–100 μ M), and poised potentials (+200 to –300 mV versus Ag/AgCl). In addition, the potential and RF concentration dependency were examined using *Geobacter sulfurreducens* PCA. Flavins are known to strongly enhance current generation in *S. oneidensis* MR-1 and *G. sulfurreducens* PCA, model EET bacteria, as a bound cofactor by forming an intermediate semi-reduced state.^{26,27,28} In contrast, HNQ and AQDS indirectly shuttle electrons between bacteria and the electrode. The basis for combining data science and microbial electrochemistry can provide a series of methods, not only as a solid basis for optimizing and enhancing BES performance but also for identifying critical parameters for biotic and abiotic complex systems.

RESULTS AND DISCUSSION

To evaluate the variation in the electrochemical signal from each well in a high-throughput system, the same sample conditions

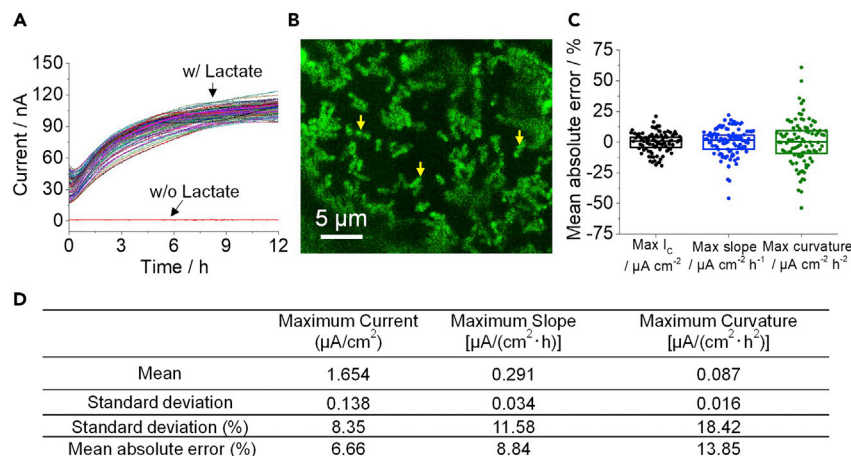


Figure 2. Low deviation current profiles in 96-well screen-printed electrochemical plate

(A) Catalytic current profiles of microbial lactate oxidation by *S. oneidensis* MR-1 in 96-well screen-printed electrochemical plate poised at +200 mV (versus Ag/AgCl).

(B) *S. oneidensis* MR-1 attached on the electrode surface observed by fluorescence microscopy. The fluorophores SYTO 9 and propidium iodide were used for assessing the vitality. The excitation/emission wavelengths used were 480/500 nm and 490/635 nm for SYTO 9 and PI, respectively. The arrows indicate the bacterial cells. Scale bar is 5 μm .

(C and D) Statistical parameters for maximum current production, slope, and curvature. Box in (C) represents mean \pm SD (n = 95).

See also Figure S1.

were measured in a 96-well three-electrode screen-printed electrochemical plate with our custom-made potentiostat, capable of measuring 20 units in parallel. *S. oneidensis* MR-1 cells were filled into all the wells at an optical density (OD) of 0.5 in an electrolyte of 200 μL , and the electrode potential was then poised at +200 mV (versus Ag/AgCl) in the anaerobic chamber at 30°C. A total of 95 out of 96 wells showed stable current generation without any significant noise (Figure 2A), indicating that manufacturing the custom potentiostat did not noticeably limit the number of effective channels. Each well showed almost identical time-current (*I*-*T*) profiles, where the current production started with a steep rise and then gradually saturated. Given that scarce current was produced in the absence of lactate as the sole electron donor (Figure 2A), the current production (I_c) in each well was attributable to the EET process associated with metabolic lactate oxidation. Furthermore, the I_c value and *I*-*T* profile were almost identical to those of the well-established commercially available potentiostat (VMP3; Biologic) (Figure S1), suggesting that potentiostatic conditions were achieved using our custom-made potentiostat. At the end of the current measurement, the working electrode (WE) surface was covered by MR-1 cells (Figure 2B), similar to conventional BES reactors.^{29,30} These results demonstrated that 96-well plates with Ag/AgCl-printed reference electrode (REs) were stable during the measurement, and *I*-*T* profiles for each well reflected the microbial activity on the bioanode.

To quantify the variation in the data, we analyzed each time profile for the maximum I_c , slope, and curvature. No baseline correction was applied, as *S. oneidensis* MR-1 cells were mixed in the electrolyte prior to addition to the electrochemical plate. Max I_c , slope, and curvature had standard deviations of approximately 8.4%, 11.6%, and 18.4%, respectively, whereas mean absolute percentage errors for each case were 6.7%, 8.8%, and 13.8%, respectively (Figures 2C and 2D). While the maximum I_c has the lowest deviation percentage from the mean, the other two also lie within the SD, which is comparable with established high-throughput systems.^{31,32} Thus, based on the data variation, our system demonstrated high reproducibility through all wells in the 96-well plate.

Next, we compared the data for some key variables (poised potential, mediator type, and concentration on I_c) with 120

different electrolytes and potentiostatic conditions in stand-alone screen-printed 576 wells (Figure S2), using six 96-well electrochemical plates, with at least n = 4 (n is the number of wells used for one condition) (Figures 3, S3A, S3B, and S3D). In all cases, I_c increased immediately upon poisoning the electrode potential. In the absence of redox mediators, maximum I_c decreased at a more negative electrode potential, suggesting that the biological effect of increasing I_c at negative potentials did not occur in our system (Figures 3 and S3B).³³ For *S. oneidensis* MR-1, an increase in I_c with an increase in mediator concentration was observed for all redox mediators at each electrode potential (Figure 3). For the positively poised electrode at +200 mV, flavins and HNQ showed relatively large currents at low (1–10 μM) and high concentrations (100 μM), respectively. This is consistent with the difference between the bound cofactor and electron shuttling mechanism reported previously.²⁸ AQDS showed the least current enhancement among the four redox mediators. A more negative electrode potential (–100 to –300 mV) resulted in a lower I_c for all tested mediators and concentrations. Meanwhile, the impact of the decrease was substantial in the case of HNQ, as shown in Figure 3; a reduction in current by seven times was observed when the poised potential was decreased gradually from +200 to –300 mV. However, the I_c decrease was only observed from –200 to –300 mV in RF and FMN, suggesting that bound cofactors and redox shuttles have different potential dependencies on the I_c performance.

To analyze such differences in potential dependency among these redox mediators in detail, we estimated the enhancement factor and its efficiency against the concentration of redox mediators (Figure 4). In some cases, I_c did not reach its peak during the electrochemical assay (Figure S3C). Therefore, we evaluated the performance in terms of the current enhancement factor using the maximum slope achieved in each case. The current enhancement factor was calculated using the following relation:

$$EF(\alpha) = \frac{S_{\max} - S_{\max,\text{ref}}}{S_{\max,\text{ref}}}, \quad (\text{Equation 1})$$

where EF is the current enhancement factor, S_{\max} is the maximum slope for each tested case with different mediators and poised

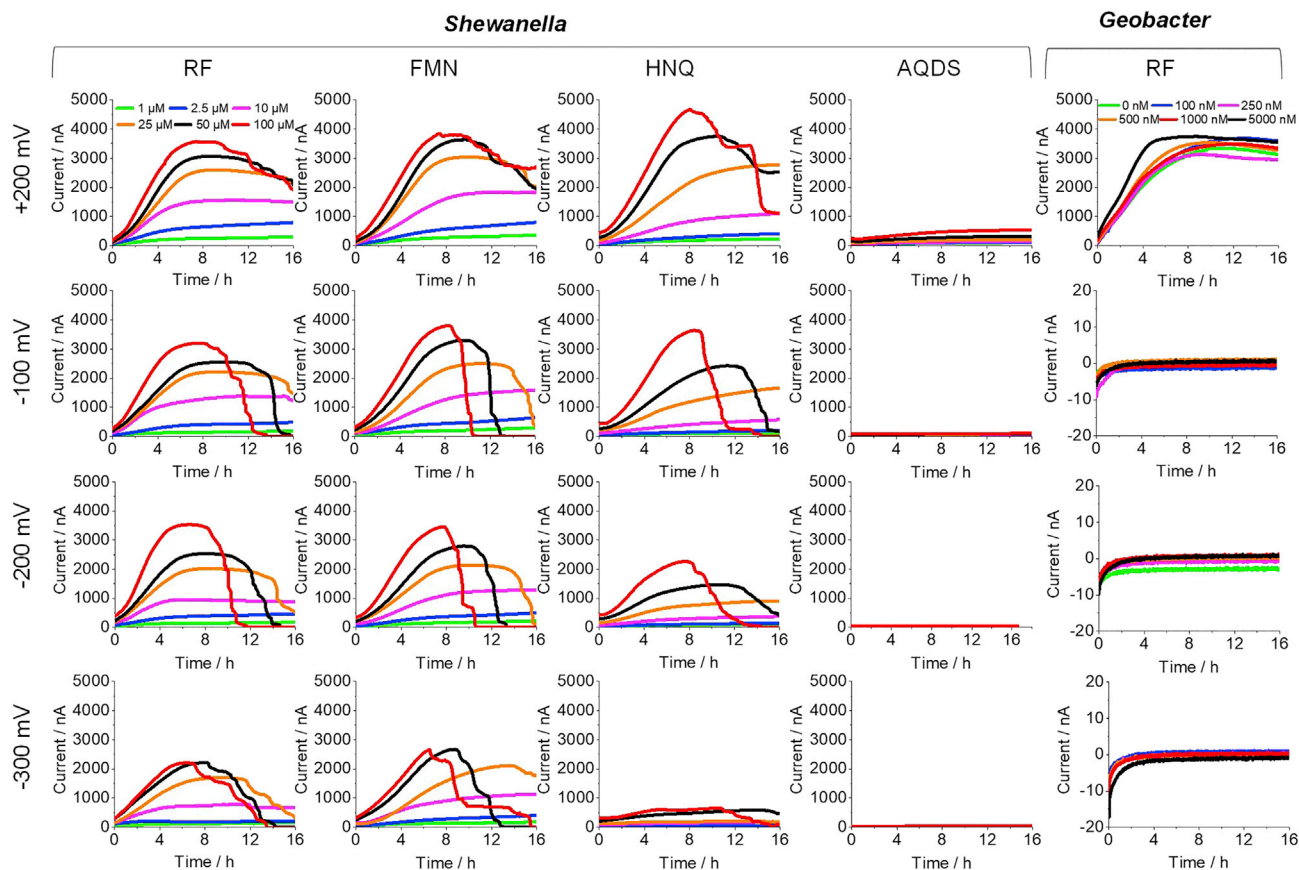


Figure 3. Impact of redox mediators and electrode potential on current production

Time-current profiles in the presence of redox mediators at different electrode potentials and concentrations in *S. oneidensis* MR-1 and *G. sulfurreducens* PCA. See also Figure S3.

potentials, and $S_{\max, \text{ref}}$ is the maximum slope of the reference cells without mediators at different poised potentials. The EF was then normalized to the added mediator's concentration to present the efficiency of each mediator molecule to enhance EET using the relation:

$$\text{Additives performance} = \frac{EF}{C}, \quad (\text{Equation 2})$$

where C is the concentration of mediators for each tested case. To plot additive performance against electron potential or mediator concentration, we conducted Bayesian estimation. Bayesian statistics were employed to explore the most efficient conditions, which were determined by the balance between additive addition and current enhancement. The basic idea of optimizing a function $f(x)$ is to determine x that maximizes $f(x)$. In Bayesian optimization, a regression model based on a Gaussian process (GP) is built for $f(x)$ from a dataset of observed x and $f(x)$. In this study, x is a two-dimensional (2D) vector composed of the poised voltage and the concentration of the mediator, and $f(x)$ is the additive performance. In this study, a scikit-learn library (i.e., sklearn GP regressor) was used to build a GP model, and a combination of three types of kernels (i.e., radial basis function, constant, and white kernels) was employed as the GP kernel. From the mean and

SD of the GP posterior predictive at x ($\mu(x)$ and $\sigma(x)$, respectively), the most probable x that might give the maximum value is estimated on the basis of an acquisition function. We used expected improvement (EI) as the acquisition function, which is defined as the following formula:

$$EI(x) = \begin{cases} (\mu(x) - f(x)_{\max} - \xi)\Phi(Z) + \sigma(x)\varphi(Z), & \sigma(x) > 0 \\ 0, & \sigma(x) = 0 \end{cases}, \quad (\text{Equation 3})$$

where

$$Z = \frac{\mu(x) - f(x)_{\max} - \xi}{\sigma(x)}. \quad (\text{Equation 4})$$

Here, $\Phi(Z)$ and $\varphi(Z)$ are the cumulative distribution function and the probability density function of Z , respectively. The parameter ξ was introduced to tune the degree of trade-off between exploration and exploitation. In this study, ξ was set at 0.01 of the SD of a dataset.

The EF profiles showed that, at lower mediator concentrations, RF and FMN exhibited higher current enhancement than HNQ and AQDS (Figure 4). For flavins, the EFs did not significantly vary with electrode potential at all concentrations (Figure 4A). High EF was observed with HNQ and AQDS,

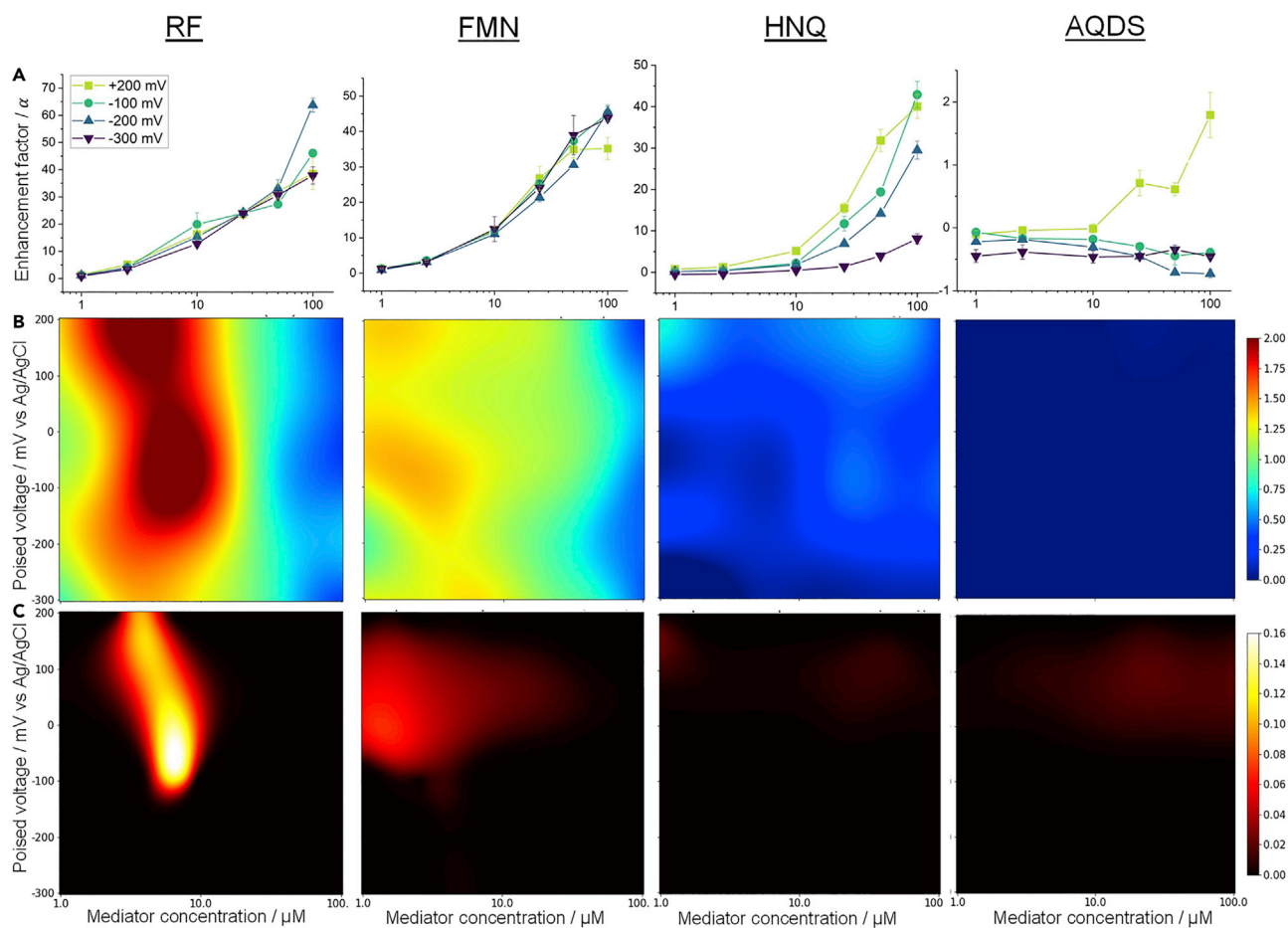


Figure 4. Additive's performance dependency on concentration and electrode potential for redox mediators

(A) Current enhancement for RF, FMN, HNQ, and AQDS additive concentration and poised electrode potentials, where enhancement factor was calculated using maximum slope against base current without any additives. Data are represented as mean \pm SEM ($n = 4$).

(B) Gaussian process regression model for the RF, FMN, HNQ, and AQDS additive performance against additive concentration and poised electrode potentials.

(C) Heatmaps for the expected improvements in RF, FMN, HNQ, and AQDS additive performance against additive concentration and poised electrode potentials. See also Figure S4.

specifically when concentration and potential were high and positive, respectively (Figure 4B). These results demonstrate that the EFs show the overall transition in the I - T profile under different conditions, as shown in Figure 3. The GP models and corresponding EIs are depicted for additive performance as 2D heatmaps, as shown in Figures 4B and 4C, with the optimized conditions for each mediator marked in these panels. The GP models effectively integrate the data into a 2D landscape, and the estimated condition for the peak performance is consistent with raw data, except for the highest performance of HNQ at 1 μM concentration, which may be associated with the amplification of error from the low current range. As shown in Figure 4C, a low (<10 μM) concentration of RF was estimated for additive peak performance, and the peak potential ranged from +200 to -100 mV. In contrast, the peak performance was localized at positive potentials from +150 to 0 mV and at HNQ concentrations greater than 50 μM . FMN and AQDS showed similar tendencies to RF and HNQ, respectively (Figures 4B and 4C).

The potential dependency of EI at peak performance concentration for each mediator showed that the EI functions of RF and FMN had one large peak and a shoulder, while those of HNQ and AQDS had one peak (Figure S4), suggesting that the two redox reactions are involved in I_c in the presence of flavins. Given that the redox potentials of bound RF and FMN, HNQ, and AQDS are closely located,^{34,35} the peak and the shoulder at around -100 mV are most likely assignable to their redox reaction with the electrode surface. Meanwhile, the main peak of flavins observed at -50 to -0 mV may also be attributable to the bound flavin cofactors in the outer membrane cytochrome (OMC). Bound flavin cofactors in OMCs mediate the single-electron redox reaction to form a semiquinone state (Sq); therefore, there are two types of redox reactions, oxidized (Ox)/Sq and Sq/hydroquinone (Hq). While the Sq/Hq coupling redox reaction was reported to mediate electron uptake from the electrode surface,³⁶ the Sq/Hq reaction may mediate anodic I_c at a negative electrode potential, more so than the Ox/Sq coupling reaction in MR-1.

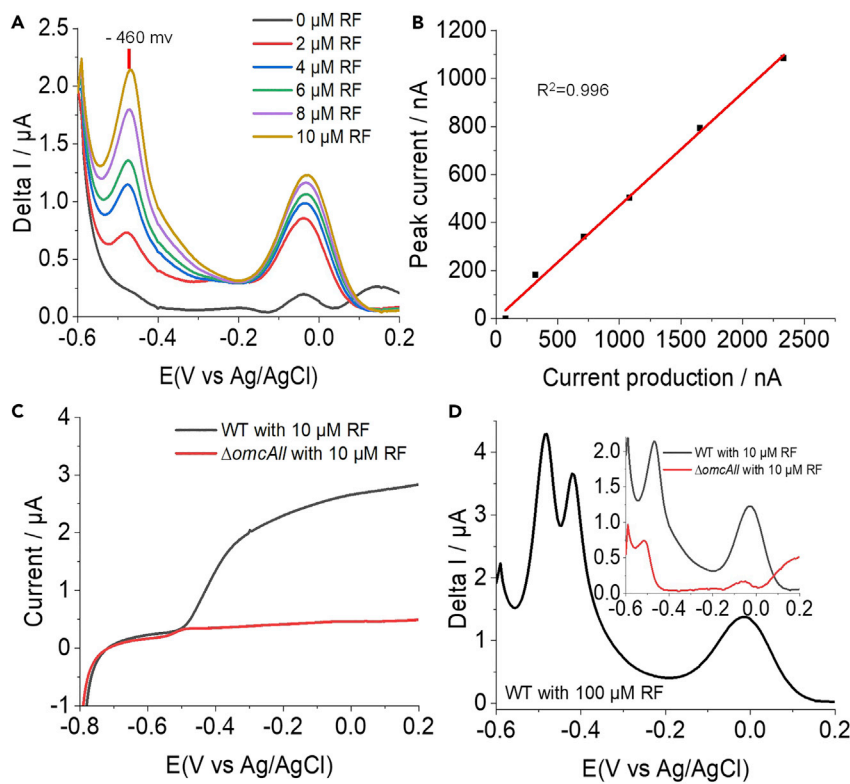


Figure 5. EET mechanism via RF as a bound cofactor in OMCs at negative potential

(A) DP voltammograms for wild type (WT) measured at different RF concentrations an hour after RF addition during current production shown in Figure S5.

(B) Plots of peak current at -460 from each DP voltammogram in (A) and I_c derived from Figure S5. The squares of the correlation coefficients were estimated by the addition of the point of origin to the obtained data.

(C) Linear sweep voltammetry for WT and $\Delta omcAll$ at $10 \mu\text{M}$ RF.

(D) DP voltammogram for WT with excess addition of RF after incubation at -200 mV (versus Ag/AgCl). Inset: DP voltammograms for WT and $\Delta omcAll$ at $10 \mu\text{M}$ RF after incubation at -200 mV (versus Ag/AgCl).

gene deletion resulted in slight I_c enhancement with increasing RF concentration. A clear decrease in the LSV and DPV signals was attributable to electron flow mediated by Sq/Hq (Figures 5C and 5D). These results further demonstrate that the Sq/Hq redox couple is the main mechanism for I_c enhancement under negative electrode poisoning conditions.

To examine the origin of I_c enhancement at the negative electrode potential in the presence of flavins, we electrochemically analyzed the presence of Sq/Hq redox coupling using differential pulse voltammetry (DPV) during potential poisoning at -200 mV at various RF concentrations (Figures 5 and S5). We observed peaks at -460 and -30 mV versus Ag/AgCl, and the peak current increased with increasing RF concentration (Figure 5A). Plots of I_c and the peak currents at -460 mV showed a linear correlation passing through the original point (Figure 5B), suggesting that both peaks are assignable to RF and that the redox signal at -460 mV attributable to RF mediates I_c under -200 mV incubation condition. Accordingly, the linear voltammetry measurement showed the onset potential of linear sweep voltammetry (LSV) started from around -0.6 V, consistent with the onset of the RF peak at -460 mV (Figure 5C). When an excessive amount of RF was added to detect the DPV signal of the free form, an additional peak at -430 mV was detected. The half-peak width ($E_{w1/2}$) for the signals at -460 and -30 mV was approximately 130 mV, and the $E_{w1/2}$ for the -430 mV peak was approximately 50 mV, which is consistent with the one- and two-electron flavin redox processes, suggesting that -460 , -430 , and -30 mV are Sq/Hq, Ox/Hq, and Ox/Sq redox reactions, respectively. This assignment is in accordance with the relative location potential for each redox couple, that is, the two-electron Ox/Hq peak is between the two redox peaks for the single-electron redox reaction, and the observation that -460 and -30 mV peak currents both increased with the added flavin concentration. Given that the Sq/Hq redox couple was stabilized in OMCs under cathodic electrode conditions in MR-1,³⁶ we used a mutant strain lacking OMCs ($\Delta omcAll$). The impact of

In contrast, such tolerance for the negative electrode potential was not observed in *G. sulfurreducens*, which is also capable of using RF as a redox cofactor in *c*-type cytochromes.²⁶ I_c was measured under the same conditions as *S. oneidensis* MR-1, except for the electrolyte medium and concentration range of RF because the dissociation constant of RF for binding OMCs was 100 times lower than that in *S. oneidensis* MR-1.²⁸ The effect of RF addition was not significant, most likely because the RF secreted or contained in the medium was sufficiently higher than the K_d value. Meanwhile, I_c was considerably suppressed at more negative electrode potential than -0.1 V (Figure 3). Assuming that the low I_c at a negative potential is caused by the dissociation of RF from OMCs, the interaction of OMCs with the negatively poised electrode may change the binding affinity of RF to OMCs. These results suggest that while the I_c capability of *G. sulfurreducens* is higher than that of *S. oneidensis* MR-1 under positively poised conditions, *S. oneidensis* MR-1 is advantageous for sustainability under conditions of anodic potential fluctuation with varying wastewater conditions. In real wastewater treatment systems, the redox potential substantially changes depending on the wastewater oxidation-reduction reactions.³⁷ For instance, the redox potential of wastewater increases in the presence of strong oxidizing agents such as hydrogen peroxide or decreases in the presence of strong reducing agents such as sodium bisulfite.³⁸ The biological oxidation-reduction reactions such as nitrification, denitrification, biological phosphorus removal, and the removal of biological oxygen demand (carbon- and hydrogen-containing compounds) also dictate the redox potential conditions. Most of these processes occur in the range of -300 to $+200$ mV, varying from anaerobic to aerobic systems.^{38,39} In this respect, the tolerance to negative electrode potential

in MR-1 is important, as among the bacteria that power BESs, *S. oneidensis* MR-1 species are widely studied for bioremediation and environmental energy recovery, owing to their robust growth in both aerobic and anaerobic environments within a wide range of redox potentials.^{40,41} However, the potential range advantage of *S. oneidensis* MR-1 has not been highlighted. This study, which captured the landscape of varying electrode potentials, not only identified the optimum additive conditions against the range of potentials but also helped elucidate the mechanism in EET. This will help real wastewater systems to control the addition of current enhancement agents in varying redox potentials for the maximum performance of BESs.

Conclusions

We demonstrated the utility of applying data science to complex bacteria and electrode interactions by successfully developing a high-throughput and low-deviation electrochemical platform. 2D landscapes of electrode potential and additive concentration generated from Bayesian estimation were primarily consistent with the bound and diffusible mechanisms in redox mediators, verifying that the quality of the database is sufficient to apply data science analysis. Furthermore, the uninvestigated region of electrode potential and mediator concentration showed an electron transfer mechanism via a bound flavin cofactor with a negatively poised electrode surface. This finding validates the database quality and provides the first example of an EET mechanism revealed by data science, highlighting the importance for the fundamental understanding of BES. By further combining it with the other data science model, our Bayesian estimation model may enable complex BES models to improve the performance of practical systems.⁴² Owing to the flexibility of the electrolyte, potential poisoning, and electrode material, the present method can be extended to many other applications in electromicrobiology—microbial fuel cells and microbial electrosynthesis, or metabolic activity sensor technologies for antibiotic drug discovery.^{43,44}

EXPERIMENTAL PROCEDURES

Resource availability

Lead contact

The lead contact is Akihiro Okamoto (okamoto.akihiro@nims.go.jp). He can be contacted for information relevant to the paper and requests for code and data.

Materials availability

This work did not produce any physical materials.

Data and code availability

All data reported in this paper will be shared by the [lead contact](#) upon request. Original codes have been deposited at Zenodo under <https://doi.org/10.5281/zenodo.7050972> and are publicly available. Any additional information required to reanalyze the data reported in this paper is available from the [lead contact](#) upon request.

Materials and methods

S. oneidensis MR-1 and *G. sulfurreducens* PCA cultivation

S. oneidensis MR-1 was cultured in 10 mL LB medium at 30°C for 20 h under aerobic conditions by picking a single colony from the

LB solid medium plate. The bacteria were washed twice with defined medium (DM) with a composition of 2.5 g NaHCO₃, 0.08 g CaCl₂, 1 g NH₄Cl, 0.2 g MgCl₂, 10 g NaCl, 7.2 g HEPES, and 0.5 g yeast extract in 1 L ultrapure water. The cells were centrifuged at 7,200 × *g* for 5 min, and the supernatant was removed. Cell pellets obtained after centrifugation were resuspended in 10 mL DM medium with 10 mM lactate (DML). Microbial cells were precultured in DML for 4 h under anaerobic conditions and then washed. Finally, the cell OD at 600 nm (OD_{600nm}) was adjusted to 0.5, using DML as the final concentration in the screen-printed electrochemical cells. $\Delta omcAII$ that referred to deletion of all outer membrane multiheme cytochrome gene homologs was constructed by deleting the genes SO1778 to SO1782, SO2931, and SO1659 from *S. oneidensis* MR-1 as described earlier.^{45,46}

G. sulfurreducens PCA freeze stock was used for inoculation of the culture in anaerobic PSN medium²⁶ supplied with 20 mM acetate and 80 mM fumarate. Cells were grown in an anaerobic bottle at 30°C for 3–4 days. Finally, the suspended cells were centrifuged (10 min at 5,000 × *g*) and washed with the PSN medium for electrochemical measurements.

Experimental plan

Screen-printed electrochemical array formed by 96 three-electrode electrochemical cells (DRP×11L (U100), Metrohm, DropSens, Tokyo, Japan) was utilized for this study. The electrochemical array was fixed at the bottom of a standard microtiter ELISA plate with 96 wells. Plastic substrate (L7.4 cm × W11 cm × H0.5 mm) was used as the base for screen printing the three electrodes. The screen-printed carbon (surface area: 7.07 mm² for each well) was used as the WE. Also, for each cell, screen-printed carbon and Ag/AgCl were used as the auxiliary (counter electrode [CE]) and RE, respectively. The backside of the plates was printed with gold-plated contact paths where 96 × 3 contacts were present, corresponding to the independent WE, CE, and RE printed for each well. Each well had a standard volume capacity of around 300–400 μL, and a working volume of 200 μL was used. After the anolyte addition, all plates were sealed with sterile aluminum seals. Since multichannel 96-well systems were used where effective volume of each cell was much less (~200 μL), it was ensured that no turbulence affected the operation by adding the medium, bacterial cells, and mediators at the beginning of experiments. Nevertheless, to probe the mechanism, control cells were included in the experiments where no exogenous small-molecule mediators were added, and hence rational analysis for elucidation of mechanism can be ensured.

In the scheme of current-time profile experiments, first, single potential amperometry measurements with our custom potentiostat using 96-well plates were compared with a commercial potentiostat (VMP3; Biologic Science Instruments, Seyssinet-Pariset, France) using screen-printed electrodes with the same electrode material and working volume as the 96-well plates. The variation in the data for 96-well plate was analyzed for the maximum *I*_c, slope, and curvature. For the multivariable impact study, five 96-well electrochemical plates were selected for *S. oneidensis* MR-1 and one plate for *G. sulfurreducens* PCA (Figure S2). For *S. oneidensis* MR-1, the first plate was checked by poisoning a single potential (versus Ag/AgCl) for two rows each, that is, the first two rows were poised at +200 mV, followed by

two rows at -100 , -200 , and -300 mV without the addition of any external mediator (Figure S2A). Four plates were tested by poisoning a single potential per plate with varying mediator concentrations (Figure S2B). DM (pH 7.8) containing lactate as the sole electron donor and DM containing each redox molecule was de-aerated by bubbling with nitrogen for 30 min. An electrolyte (200 μ L) was then added to each electrochemical cell containing 10 mM lactate and the desired concentrations of flavin analogs and quinones (1–100 μ M), and MR-1 cell suspensions with $OD_{600nm} = 0.5$. PLATEMASTER P220 (Gilson, Middleton, WI, USA) was used for pipetting volumes of 2–220 μ L for high-throughput manual pipetting of 96 wells. For *G. sulfurreducens* PCA, a single plate was used to study 24 conditions (Figure S2C). This includes four poised potential conditions (+200, -100 , -200 , and -300 mV) and six RF mediator concentrations (0, 100, 250, 500, 1,000, and 5,000 nM). All the experiments were performed in an anaerobic chamber filled with 100% N_2 . The chamber was also intermittently filled with H_2 gas mix (5% or less) that reacted with a palladium catalyst to remove O_2 by forming a H_2O molecule. The temperature was maintained at $30^\circ C$ during the measurements.

At the end of bioelectrochemical experiment, *S. oneidensis* MR-1 attached on the electrode surface were observed by fluorescence microscopy. The fluorophores SYTO 9 and propidium iodide (PI) were used for assessing the vitality. The excitation/emission wavelengths used were 480/500 nm and 490/635 nm for SYTO 9 and PI, respectively. Fluorescein isothiocyanate (FITC) and Texas Red (TxR) were used as filters.

SUPPLEMENTAL INFORMATION

Supplemental information can be found online at <https://doi.org/10.1016/j.patter.2022.100610>.

ACKNOWLEDGMENTS

The financial support for this work was provided by a Grant-in-Aid for Research from the Japan Society for Promotion of Science KAKENHI (grant nos. 20H05590 and 22H02265) and the Japan Agency for Medical Research and Development (19gm6010002h0004 and 21he0322002j0002). This work was also supported by JST, PRESTO grant number JPMJPR19H1, Japan, and by JAEA Nuclear Energy S&T and Human Resource Development Project through concentrating wisdom grant number JPJA20P20333393.

AUTHOR CONTRIBUTIONS

Conceptualization, W.M. and A.O.; methodology, W.M., W.H., and A.O.; formal analysis, W.M., G.I., and A.O.; investigation, W.M., W.H., X.L., and A.O.; writing – original draft, W.M., W.H., X.L., G.I., and A.O.; writing – review & editing, G.I. and A.O.; funding acquisition, A.O.; resources, A.O.; supervision, A.O.

DECLARATION OF INTERESTS

A.O. filed a patent application for the high-throughput device.

Received: June 4, 2022

Revised: August 24, 2022

Accepted: September 21, 2022

Published: October 19, 2022

REFERENCES

1. Logan, B.E., Rossi, R., Ragab, A., and Saikaly, P.E. (2019). Electroactive microorganisms in bioelectrochemical systems. *Nat. Rev. Microbiol.* *17*, 307–319. <https://doi.org/10.1038/s41579-019-0173-x>.
2. Shi, L., Dong, H., Reguera, G., Beyenal, H., Lu, A., Liu, J., Yu, H.-Q., and Fredrickson, J.K. (2016). Extracellular electron transfer mechanisms between microorganisms and minerals. *Nat. Rev. Microbiol.* *14*, 651–662. <https://doi.org/10.1038/nrmicro.2016.93>.
3. Ziara, R.M.M., Dvorak, B.I., and Subbiah, J. (2018). Chapter 7 - sustainable waste-to-energy technologies: bioelectrochemical systems. In *Sustainable Food Waste-to-Energy Systems*, T.A. Trabold and C.W. Babbitt, eds. (Academic Press), pp. 111–140.
4. Liang, P., Wang, H., Xia, X., Huang, X., Mo, Y., and Cao, X. (2011). Carbon nanotube powders as electrode modifier to enhance the activity of anodic biofilm in microbial fuel cells. *Biosensors and Bioelectronics* *26*, 3000–3004. <https://doi.org/10.1016/j.bios.2010.12.002>.
5. Watson, V.J., Saito, T., Hickner, M.A., and Logan, B.E. (2011). Polymer coatings as separator layers for microbial fuel cell cathodes. *Journal of Power Sources* *196*, 3009–3014. <https://doi.org/10.1016/j.jpowsour.2010.11.105>.
6. Jiang, D., Li, X., Raymond, D., Mooradain, J., and Li, B. (2010). Power recovery with multi-anode/cathode microbial fuel cells suitable for future large-scale applications. *International Journal of Hydrogen Energy* *35*, 8683–8689. <https://doi.org/10.1016/j.ijhydene.2010.04.136>.
7. Logan, B.E. (2010). Scaling up microbial fuel cells and other bioelectrochemical systems. *Appl. Microbiol. Biotechnol.* *85*, 1665–1671. <https://doi.org/10.1007/s00253-009-2378-9>.
8. Gadkari, S., Fontmorin, J.-M., Yu, E., and Sadhukhan, J. (2020). Influence of temperature and other system parameters on microbial fuel cell performance: numerical and experimental investigation. *Chem. Eng. J.* *388*, 124176.
9. Chen, S., Patil, S.A., Brown, R.K., and Schröder, U. (2019). Strategies for optimizing the power output of microbial fuel cells: Transitioning from fundamental studies to practical implementation. *Applied Energy* *233–234*, 15–28. <https://doi.org/10.1016/j.apenergy.2018.10.015>.
10. Ahmadi, M., Ziatdinov, M., Zhou, Y., Lass, E.A., and Kalinin, S.V. (2021). Machine learning for high-throughput experimental exploration of metal halide perovskites. *Joule* *5*, 2797–2822. <https://doi.org/10.1016/j.joule.2021.10.001>.
11. An, N.G., Kim, J.Y., and Vak, D. (2021). Machine learning-assisted development of organic photovoltaics via high-throughput in situ formulation. *Energy Environ. Sci.* *14*, 3438–3446. <https://doi.org/10.1039/D1EE00641J>.
12. Zhong, M., Tran, K., Min, Y., Wang, C., Wang, Z., Dinh, C.-T., De Luna, P., Yu, Z., Rasouli, A.S., Brodersen, P., et al. (2020). Accelerated discovery of CO₂ electrocatalysts using active machine learning. *Nature* *581*, 178–183. <https://doi.org/10.1038/s41586-020-2242-8>.
13. Du, X., Lüer, L., Heumueller, T., Wagner, J., Berger, C., Osterrieder, T., Wortmann, J., Langner, S., Vongsaysy, U., Bertrand, M., et al. (2021). Elucidating the full potential of OPV materials utilizing a high-throughput robot-based platform and machine learning. *Joule* *5*, 495–506. <https://doi.org/10.1016/j.joule.2020.12.013>.
14. Molderez, T.R., Zhang, X., Rabaey, K., and Verhelst, M. (2019). A current-driven six-channel potentiostat for rapid performance characterization of microbial electrolysis cells. *IEEE Trans. Instrum. Meas.* *68*, 4694–4702. <https://doi.org/10.1109/TIM.2019.2898049>.
15. Vergani, M., Carminati, M., Ferrari, G., Landini, E., Caviglia, C., Heiskanen, A., Comminges, C., Zór, K., Sabourin, D., Dufva, M., et al. (2012). Multichannel bipotentiostat integrated with a microfluidic platform for electrochemical real-time monitoring of cell cultures. *IEEE Trans. Biomed. Circuits Syst.* *6*, 498–507. <https://doi.org/10.1109/TBCAS.2012.2187783>.
16. Tahernia, M., Mohammadifar, M., Gao, Y., Panmanee, W., Hassett, D.J., and Choi, S. (2020). A 96-well high-throughput, rapid-screening platform

- of extracellular electron transfer in microbial fuel cells. *Biosens. Bioelectron.* *162*, 112259.
17. Call, D.F., and Logan, B.E. (2011). A method for high throughput bioelectrochemical research based on small scale microbial electrolysis cells. *Biosens. Bioelectron.* *26*, 4526–4531. <https://doi.org/10.1016/j.bios.2011.05.014>.
 18. Molderez, T.R., Prévosteau, A., Ceyskens, F., Verhelst, M., and Rabaey, K. (2021). A chip-based 128-channel potentiostat for high-throughput studies of bioelectrochemical systems: optimal electrode potentials for anodic biofilms. *Biosens. Bioelectron.* *174*, 112813.
 19. Szydlowski, L., Ehlich, J., Goryanin, I., and Pasternak, G. (2021). High-throughput 96-well bioelectrochemical platform for screening of electroactive microbial consortia. *Chemical Engineering Journal* *131692*. <https://doi.org/10.1016/j.cej.2021.131692>.
 20. Tsompanas, M.-A., You, J., Wallis, L., Greenman, J., and Ieropoulos, I. (2019). Artificial neural network simulating microbial fuel cells with different membrane materials and electrode configurations. *Journal of Power Sources* *436*, 226832. <https://doi.org/10.1016/j.jpowsour.2019.226832>.
 21. Lesnik, K.L., and Liu, H. (2017). Predicting microbial fuel cell biofilm communities and bioreactor performance using artificial neural networks. *Environ. Sci. Technol.* *51*, 10881–10892. <https://doi.org/10.1021/acs.est.7b01413>.
 22. Zhang, X., Li, X., Zhao, X., Li, Y., and Ieropoulos, I.A. (2019). Evaluation of artificial neural network algorithms for predicting the effect of the urine flow rate on the power performance of microbial fuel cells. *RSC Adv.* *213*, 118806–118823. <https://doi.org/10.1039/C9RA03605A>.
 23. Zhang, X., Li, X., Zhao, X., and Li, Y. (2019). Factors affecting the efficiency of a bioelectrochemical system: a review. *RSC Advances* *9*, 19748–19761. <https://doi.org/10.1039/C9RA03605A>.
 24. Martinez, C.M., and Alvarez, L.H. (2018). Application of redox mediators in bioelectrochemical systems. *Biotechnol. Adv.* *36*, 1412–1423.
 25. Kumar, A., Hsu, L.H.-H., Kavanagh, P., Barrière, F., Lens, P.N.L., Lapinsonnière, L., Lienhard V, J.H., Schröder, U., Jiang, X., and Leech, D. (2017). The ins and outs of microorganism–electrode electron transfer reactions. *Nat. Rev. Chem.* *1*, 0024. <https://doi.org/10.1038/s41570-017-0024>.
 26. Okamoto, A., Saito, K., Inoue, K., Neelson, K.H., Hashimoto, K., and Nakamura, R. (2014). Uptake of self-secreted flavins as bound cofactors for extracellular electron transfer in *Geobacter* species. *Energy Environ. Sci.* *7*, 1357–1361.
 27. Okamoto, A., Hashimoto, K., Neelson, K.H., and Nakamura, R. (2013). Rate enhancement of bacterial extracellular electron transport involves bound flavin semiquinones. *Proc. Natl. Acad. Sci. USA* *110*, 7856–7861. <https://doi.org/10.1073/pnas.1220823110>.
 28. Okamoto, A., Nakamura, R., Neelson, K.H., and Hashimoto, K. (2014). Bound flavin model suggests similar electron-transfer mechanisms in *Shewanella* and *Geobacter*. *Chemelectrochem* *1*, 1808–1812. <https://doi.org/10.1002/celec.201402151>.
 29. Patil, S.A., Górecki, K., Hägerhäll, C., and Gorton, L. (2013). Cisplatin-induced elongation of *Shewanella oneidensis* MR-1 cells improves microbe–electrode interactions for use in microbial fuel cells. *Energy Environ. Sci.* *6*, 2626–2630. <https://doi.org/10.1039/C3EE41974F>.
 30. Zhao, C.-e., Wu, J., Kjelleberg, S., Loo, J.S.C., and Zhang, Q. (2015). Employing a flexible and low-cost polypyrrole nanotube membrane as an anode to enhance current generation in microbial fuel cells. *Small* *11*, 3440–3443.
 31. Riba, J., Gleichmann, T., Zimmermann, S., Zengerle, R., and Koltay, P. (2016). Label-free isolation and deposition of single bacterial cells from heterogeneous samples for clonal culturing. *Sci. Rep.* *6*, 32837. <https://doi.org/10.1038/srep32837>.
 32. Matsui, T.S., Wu, H., and Deguchi, S. (2018). Deformable 96-well cell culture plate compatible with high-throughput screening platforms. *PLoS One* *13*, e0203448. <https://doi.org/10.1371/journal.pone.0203448>.
 33. Hirose, A., Kasai, T., Aoki, M., Umemura, T., Watanabe, K., and Kouzuma, A. (2018). Electrochemically active bacteria sense electrode potentials for regulating catabolic pathways. *Nat. Commun.* *9*, 1083. <https://doi.org/10.1038/s41467-018-03416-4>.
 34. Shi, Z., Zachara, J.M., Shi, L., Wang, Z., Moore, D.A., Kennedy, D.W., and Fredrickson, J.K. (2012). Redox reactions of reduced flavin mononucleotide (FMN), riboflavin (RBF), and anthraquinone-2, 6-disulfonate (AQDS) with ferrihydrite and lepidocrocite. *Environ. Sci. Technol.* *46*, 11644–11652. <https://doi.org/10.1021/es301544b>.
 35. Wu, Y., Liu, T., Li, X., and Li, F. (2014). Exogenous electron shuttle-mediated extracellular electron transfer of *Shewanella putrefaciens* 200: electrochemical parameters and thermodynamics. *Environ. Sci. Technol.* *48*, 9306–9314. <https://doi.org/10.1021/es5017312>.
 36. Okamoto, A., Hashimoto, K., and Neelson, K.H. (2014). Flavin redox bifurcation as a mechanism for controlling the direction of electron flow during extracellular electron transfer. *Angew. Chem. Int. Ed. Engl.* *53*, 10988–10991.
 37. Li, B., and Bishop, P.L. (2004). Oxidation-reduction potential changes in aeration tanks and microprofiles of activated sludge floc in medium- and low-strength wastewaters. *Water Environ. Res.* *76*, 394–403. <https://doi.org/10.2175/106143004x151662>.
 38. Higgins, P. (2008). ORP Management in Wastewater as an Indicator of Process Efficiency (YSI). [ysi.com/media/pdfs/A567-ORP-Management-in-Wastewater-as-an-Indicator-of-Process-Efficiency.pdf](https://www.ysi.com/media/pdfs/A567-ORP-Management-in-Wastewater-as-an-Indicator-of-Process-Efficiency.pdf).
 39. Goncharuk, V.V., Bagrii, V.A., Mel'nik, L.A., Chebotareva, R.D., and Bashtan, S.Y. (2010). The use of redox potential in water treatment processes. *J. Water Chem. Technol.* *32*, 1–9. <https://doi.org/10.3103/S1063455X10010017>.
 40. Lovley, D.R. (2006). Bug juice: harvesting electricity with microorganisms. *Nat. Rev. Microbiol.* *4*, 497–508. <https://doi.org/10.1038/nrmicro1442>.
 41. Verma, J., Kumar, D., Singh, N., Katti, S.S., and Shah, Y.T. (2021). Electricigens and microbial fuel cells for bioremediation and bioenergy production: a review. *Environ. Chem. Lett.* *19*, 2091–2126. <https://doi.org/10.1007/s10311-021-01199-7>.
 42. Shahriari, B., Swersky, K., Wang, Z., Adams, R.P., and de Freitas, N. (2016). Taking the human out of the loop: a review of bayesian optimization. *Proc. IEEE* *104*, 148–175. <https://doi.org/10.1109/JPROC.2015.2494218>.
 43. Naradasu, D., Guionet, A., Miran, W., and Okamoto, A. (2020). Microbial current production from *Streptococcus mutans* correlates with biofilm metabolic activity. *Biosens. Bioelectron.* *162*, 112236.
 44. Miran, W., Naradasu, D., and Okamoto, A. (2021). Pathogens electrogenicity as a tool for in-situ metabolic activity monitoring and drug assessment in biofilms. *iScience* *24*, 102068. <https://doi.org/10.1016/j.isci.2021.102068>.
 45. Bücking, C., Popp, F., Kerzenmacher, S., and Gescher, J. (2010). Involvement and specificity of *Shewanella oneidensis* outer membrane cytochromes in the reduction of soluble and solid-phase terminal electron acceptors. *FEMS Microbiol. Lett.* *306*, 144–151. <https://doi.org/10.1111/j.1574-6968.2010.01949.x>.
 46. Rowe, A.R., Rajeev, P., Jain, A., Pirbadian, S., Okamoto, A., Gralnick, J.A., et al. (2018). Tracking Electron Uptake from a Cathode into *Shewanella* Cells: Implications for Energy Acquisition from Solid-Substrate Electron Donors. *mBio* *9*, e02203–e02217. <https://doi.org/10.1128/mBio.02203-17>.